Analyst

PAPER

View Article Online
View Journal | View Issue

Cite this: *Analyst*, 2015, **140**, 4260

Green synthesis of multifunctional carbon dots from coriander leaves and their potential application as antioxidants, sensors and bioimaging agents†

Abhay Sachdev[a] and P. Gopinath*[a,b]

Received 7th March 2015,
Accepted 17th April 2015

DOI: 10.1039/c5an00454c

www.rsc.org/analyst

In the present study, a facile one-step hydrothermal treatment of coriander leaves for preparing carbon dots (CDs) has been reported. Optical and structural properties of the CDs have been extensively studied by UV-visible and fluorescence spectroscopic, microscopic (transmission electron microscopy, scanning electron microscopy) and X-ray diffraction techniques. Surface functionality and composition of the CDs have been illustrated by elemental analysis and Fourier transform infrared spectroscopy (FTIR). Quenching of the fluorescence of the CDs in the presence of metal ions is of prime significance, hence CDs have been used as a fluorescence probe for sensitive and selective detection of Fe^{3+} ions. Eventually, biocompatibility and bioimaging aspects of CDs have been evaluated on lung normal (L-132) and cancer (A549) cell lines. Qualitative analysis of cellular uptake of CDs has been pursued through fluorescence microscopy, while quantitative analysis using a flow cytometer provided an insight into the concentration and cell-type dependent uptake of CDs. The article further investigates the antioxidant activity of CDs. Therefore, we have validated the practicality of CDs obtained from a herbal carbon source for versatile applications.

1. Introduction

In the quest for developing environmentally benign and biocompatible fluorescent nanomaterials, carbon dots (CDs) have gradually emerged as superior alternatives to heavy metal based quantum dots (QDs) for similar applications.[1–3] Ever since the existence of CDs was realized a few years ago, they have received tremendous attention owing to their unique, desirable properties such as wavelength-tuneable emission, photostability, aqueous solubility, low toxicity and functionalizability.[1,2] Because of their distinct properties and benefits, CDs have been utilized for a host of prospective applications in the area of bioimaging,[4,5] gene/drug delivery,[6,7] sensing[8–11] and catalysis.[12] A recent report from our laboratory suggests the implication of surface passivation for enhancing the brightness of CDs for bioimaging applications.[4] In this context, a large number of organic moieties, such as polyethylene glycol (PEG), polyethyleneimine (PEI), and 4,7,10-trioxa-1,13-tridecanediamine (TTDDA) have been frequently used as passivating agents, which is a complex process.[4,5,13,14]

Lately, a variety of approaches namely microwave irradiation,[5,8,9,13] hydrothermal treatment,[4,14–18] laser ablation,[19] arc discharge[20] and chemical oxidation[21] have been adopted for the synthesis of CDs. Amongst these, laser ablation and arc discharge require sophisticated and expensive energy-consuming equipment, while chemical oxidation relies on the use of strong acids. Microwave irradiation provides an easy way of synthesizing CDs within minutes, but the technique suffers from the limitation of uncontrollable reaction conditions. The hydrothermal route is mostly preferred because the technique offers simplicity, controlled reaction conditions, rapidity and cost effectiveness. Despite several advancements in the field of CDs synthesis, use of stringent reaction conditions, toxic precursors and post synthetic steps for surface passivation are often complicated and hinder their wide applications. Green synthesis of CDs is a highly attractive research topic, which exploits the use of natural, renewable carbon precursors. Nevertheless, it is always exciting to explore the green sources for CDs because these are inexpensive, clean, nontoxic and easily accessible. Accordingly, the use of grape juice,[15] lime juice,[16] milk,[17] potato,[18] orange juice,[22] plant leaves,[23,24] oats[25] and even waste biomass[26] have been reported as natural green sources for CDs. However, the key

[a]*Nanobiotechnology Laboratory, Centre for Nanotechnology, Indian Institute of Technology Roorkee, Roorkee, Uttarakhand-247667, India.*
E-mail: pgopifnt@iitr.ernet.in, genegopi@gmail.com; Fax: +91-1332-273560; Tel: +91-1332-285650
[b]*Department of Biotechnology, Indian Institute of Technology Roorkee, Roorkee, Uttarakhand-247667, India*

†Electronic supplementary information (ESI) available. See DOI: 10.1039/c5an00454c

challenge remains to produce CDs with high quantum yields in ample amounts by using simple one-step methodologies.

By taking into account all the above considerations, we report herein a green synthetic approach for synthesizing CDs from coriander leaves by one-step hydrothermal mediated synthesis. This methodology is cost-effective, less time-consuming and uses water as a solvent. Importantly, no additional surface passivation agent was required and coriander leaves solely served as the carbon source and the passivation agent for CDs. Coriander leaves are edible and naturally contain carbohydrate and proteins which are abundant in carbon, nitrogen and oxygen elements. Consequently, the formation of CDs may involve dehydration and carbonization of the coriander leaves followed by *in situ* surface passivation under high temperature and pressure during the hydrothermal treatment.[4,15,26] Fortunately, the as-prepared CDs have sufficient quantum yield, favourable for further applications. Besides, a detailed analysis of the optical and physicochemical properties of CDs has been presented in detail. Apart from this, our study encompasses the multifunctional aspects of CDs such as potential antioxidants and selective ion detection probes. To demonstrate the bioimaging potential of CDs *in vitro*, A549 (human lung adenocarcinoma) cells and L-132 (human normal lung epithelial) cells were selected as model systems, since lung cancer is the second-most prevalent type of cancer in the world.[27]

2. Experimental section

2.1 Materials

Fresh coriander leaves were purchased from a local grocery shop and was washed thoroughly before use. Quinine sulphate was purchased from Loba Chemie Pvt. Ltd, India. Cobalt(II) nitrate hexahydrate, ferrous sulphate heptahydrate, ferric chloride anhydrous, zinc nitrate hexahydrate, lead(II) nitrate and mercury(II) chloride were purchased from Himedia Laboratories Pvt. Ltd, India. Copper sulphate, calcium chloride, and magnesium chloride were purchased from Sisco Research Laboratories (SRL) Pvt. Ltd, India. Silver nitrate and cadmium acetate were supplied by Merck Ltd, India. Nickel(II) acetate tetrahydrate was purchased from Sigma Aldrich, USA. Solvents such as *N*-dimethylformamide (DMF), and hydrochloric acid (HCl) were purchased from Rankem Pvt. Ltd, India; dimethylsulfoxide (DMSO) and methanol were purchased from SD-Fine Chemicals Limited (SDFCL), India, while sodium hydroxide (NaOH) and 2,2-diphenyl-1-picrylhydrazyl (DPPH) were supplied by Himedia Laboratories Pvt. Ltd, India. 3-(4,5-Dimethylthiazol-2-yl)-2,5-diphenyl-tetrazolium bromide (MTT) dye was purchased from Amresco, USA. All the solutions were prepared in ultrapure water.

2.2 Synthesis of CDs

The preparation of CDs is as follows: 5 g of coriander leaves were chopped very finely and dissolved in 40 mL of distilled water. The solution was then transferred to an 80 mL vessel and then underwent hydrothermal treatment for 4 h at 240 °C. The solution was allowed to cool naturally and the large black insoluble carbonaceous particles were removed by filtration through a 0.22 μm filter membrane. Finally, the volume of the solution was adjusted with water to obtain CDs at a concentration of 10 mg mL^{-1} for further characterization and use.

2.3 Characterization techniques for CDs

Fluorescence spectral recording and emission measurements were carried out using a Hitachi F-4600 fluorescence spectrophotometer and a Biotek, Cytation 3 multi-mode microplate reader (for ion sensing experiments), respectively. Absorbance spectra were recorded by using a Lasany LI-2800 UV-vis double beam spectrophotometer. Transmission electron microscopy (TEM) images were acquired on a FEI Technai G2 microscope operating at 200 kV by drop casting an appropriate dilution of CDs onto the carbon-coated copper grids. Particle size analysis was done using Image J software. Elemental mapping of CDs was performed using a Carl Zeiss Ultra Plus field emission scanning electron microscopy (FE-SEM) coupled with energy dispersive X-ray spectrometry (EDS) facility. X-ray diffraction (XRD) patterns of CDs were obtained using a Bruker AXS D8 advance powder X-ray diffractometer with Cu-Kα radiation, λ = 1.5406 Å in the range of 0°–90° at a scan rate of 1° min^{-1}. Elemental analysis was carried out on an Elementar Analysensysteme GmbH variomicro CHNS. Identification of functional groups was done using a Thermo Nicolet FTIR using KBR pellets. Zeta potential and DLS measurements were conducted using a Malvern, Nano ZS 90 zetasizer. Thermo gravimetric analysis (TGA) was performed using a TG/DTA SII 6300 EXSTAR thermal analyzer by heating 10 mg of CDs under the flow of N_2 gas to 860 °C at the rate of 5 °C min^{-1}. Fluorescence decay curves were recorded using a Horiba Jobin Yvon "Fluoro Cube Fluorescence Lifetime System" equipped with a Nano LED (635 nm) source. The decay curve analysis and lifetime calculation were done by IBH decay analysis v 6.1 software.

2.4 Determination of antioxidant activity

The antioxidant potential of CDs was measured by 2,2-diphenyl-1-picrylhydrazyl (DPPH) free radical assay with few modifications.[28–30] Precisely, different concentrations of CDs were added to 0.5 mL of 50 μM methanolic solution of DPPH. The final volume of all the solutions was 0.6 mL. The samples along with appropriate controls were incubated for 30 minutes in the dark environment. 0.1 mL aliquots of all the samples were added to 96-well plate. The change in absorbance of DPPH was measured at 517 nm using a multi-mode microplate reader (Biotek, Cytation 3). The percentage radical scavenging activity of CDs was calculated using the following formula:

$$\%\ \text{Scavenging activity} = (AD_{517} - AS_{517}/AD_{517}) \times 100\%$$

where AD and AS are the absorbance of the DPPH solution (without CDs) and sample solution (with CDs), respectively.

2.5 Procedure for ion sensing

All the metal ion stock solutions were prepared from their respective salts. Aqueous solutions of these metal ions were

further diluted with deionized water to obtain a final concentration of 60 μM. Each of the metal ion solution was mixed with CDs (10 μL, 0.1 mg mL^{-1}), stirred and incubated for 15 min at room temperature. Aliquots were transferred to a 96-well black plate and fluorescence measurements were done. For Fe^{3+} sensing, similar steps were followed. In a typical assay, 10 μL of CDs solution was added to 1 mL Fe^{3+} salt solutions of different concentrations. The fluorescence intensity and spectra were recorded at an excitation wavelength of 320 nm.

2.6 Cell culture

A549 (human lung adenocarcinoma) cells and L-132 (human normal lung epithelial) cells were obtained from National Centre for Cell Sciences, Pune, India. These cell lines were maintained at 5% CO_2 in a humidified incubator at 37 °C. The cells were cultured in Dulbecco's modified Eagle's medium (DMEM, Sigma-Aldrich) supplemented with 10% v/v fetal bovine serum and 1% penicillin–streptomycin solution (Sigma-Aldrich, USA).

2.7 MTT assay

Cellular toxicity was determined by measuring the activity of mitochondrial enzymes in live cells to transform the soluble, yellow MTT solution to an insoluble, purple formazan product. The cells were cultured in 96-well tissue culture plates at a density of 10^4 cells per well. After attachment, the cells were incubated with a medium containing different doses of CDs for 12 h. Subsequently after incubation, the medium from each well was removed and the cells were washed in phosphate-buffered solution (PBS). A fresh medium containing 10 μL of 5 mg mL^{-1} solution of MTT was added to each well and kept for 4 h. The medium was removed and 150 μL of DMSO was then added to dissolve the formazan crystals. The absorbance of each well was recorded at 570 nm using a multimode microplate reader (Biotek, Cytation 3). The untreated cells were used as controls for calculating the relative percentage cell viability [mean (%) ± SEM, $n = 3$] from the following equation:

$$\%\ \text{Cell viability} = (A_{570}\ \text{in treated sample}/A_{570}\ \text{in control sample}) \times 100\%$$

2.8 Bioimaging and cellular uptake

For exploring the bioimaging potential of CDs, A549 and L-132 cells were seeded at a density of 2×10^5 in 2 mL DMEM in 3 cm culture dishes. Consequently, a fresh medium containing 0.5 mg mL^{-1} filtered sterilized CDs was added to the respective dishes and incubated for 12 h. After washing with PBS twice, the cells were imaged using a fluorescence inverted microscope. Cellular distribution of CDs was studied in a similar manner, except that the cells were stained with 3 μL of Hoechst 33342 (working concentration 10 mg mL^{-1}) and incubated for 15 min before imaging the cells under fluorescence microscope. All the fluorescence microscopic images were acquired by using a EVOS® FL Color, AMEFC 4300 inverted microscope equipped with bright field, DAPI (excitation 360 nm, emission 447 nm), GFP (excitation 470 nm, emission 525 nm), light cubes, respectively. For flow cytometry, CDs treated and untreated A549 and L-132 cells were trypsinized, collected and resuspended in PBS for analysis. The cell suspension was then analyzed by using a flow cytometer (Amnis Flowsight) under 488 nm excitation laser, by selecting the appropriate channel. Collected data (10 000 events per sample) were analyzed using Amnis Ideas software.

3. Results and discussion

Coriander is a natural herb which is commonly being used around the world as a condiment, abundant in carbon, oxygen and nitrogen elements. Moreover, coriander leaves can act as an excellent green and natural precursor material for the synthesis of CDs without the aid of any additional passivating agent. The successful preparation of such CDs has been carried out by a one-step hydrothermal treatment, which produced a yellow or light brown aqueous solution, indicating successful carbonization of the coriander leaves. Bright green luminescence under UV light further implied the formation of CDs (Fig. 1(A)). The aqueous solution of CDs shows two absorption peaks at 273 nm and 320 nm which were attributed to π–π* transition of C=C bonds and n–π* transition of C=O bonds in CDs (Fig. 1(B)).[4,5,26] On the other hand, fluorescence spectra depicted an excitation dependent behaviour. With an increase in excitation wavelength from 320 nm to 480 nm, the maximum emission shifted from 400 nm to 510 nm along with a concurrent decrease in emission intensity (Fig. 1(C)). The quantum yield of CDs was determined to be 6.48% using quinine sulphate as a reference (Table S1†).[4,5] TEM images revealed uniform black dots with near-spherical morphology (Fig. 2(A)). The average mean diameter of the CDs was 2.387 with size distribution ranging from 1.5 to 2.98 nm, as estimated from statistical distributions (Fig. 2(B)). At the same time, the SAED pattern of the CDs showed diffused rings, suggesting an amorphous carbon phase (Fig. S1†). Due to small size, low contrast and amorphous nature of CDs, high resolution TEM images could not be obtained. The aqueous suspension of CDs had an average hydrodynamic diameter of 4.158 nm, slightly more than the mean dried-state diameter as illustrated by TEM results (Fig. 2(C)). EDS elemental mapping distributions further indicated the presence of carbon (C), nitrogen (N) and oxygen (O) elements in CDs (Fig. 2(D)). These correspond to the distribution of the functional groups formed on the surface of CDs. In addition, XRD pattern depicted a broad amorphous hump at $2\theta = 21.5°$ along with a weak peak at $2\theta = 38.5°$ corresponding to (002) and (101) planes of amorphous carbon in accordance with the SAED results (Fig. 3(A)).[4,23] Elemental composition of CDs was elucidated by CHN analyzer, confirming the presence of 50.8% C, 5.3% H, 4.07% N and 39.83% O (calculated). Higher C and O content and lesser N content indicated that these particles were predominantly composed of carbon and oxygen containing functional groups along with few nitrogen containing

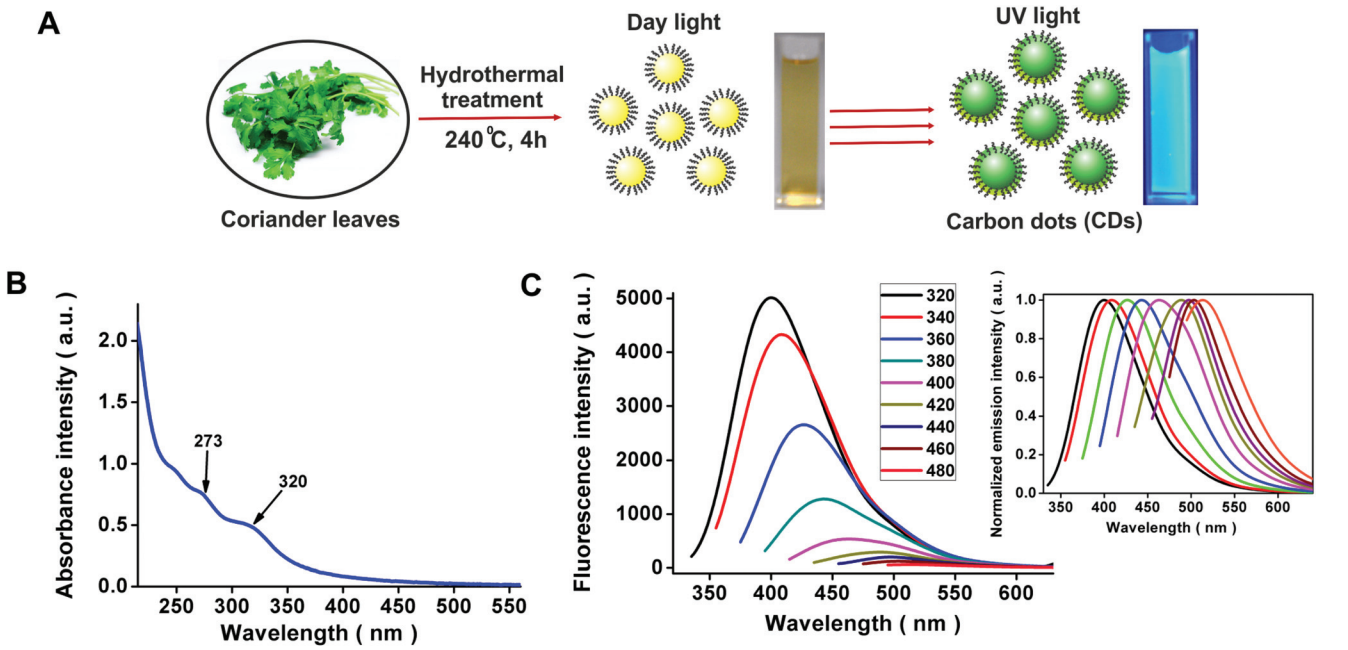

Fig. 1 (A) Schematic illustration depicting one-step synthesis of CDs from coriander leaves. (B) UV-vis absorption spectrum of CDs. (C) Fluorescence emission spectra of CDs at different excitation wavelengths ranging from 320 nm to 480 nm with increments of 20 nm (inset: normalized emission intensity).

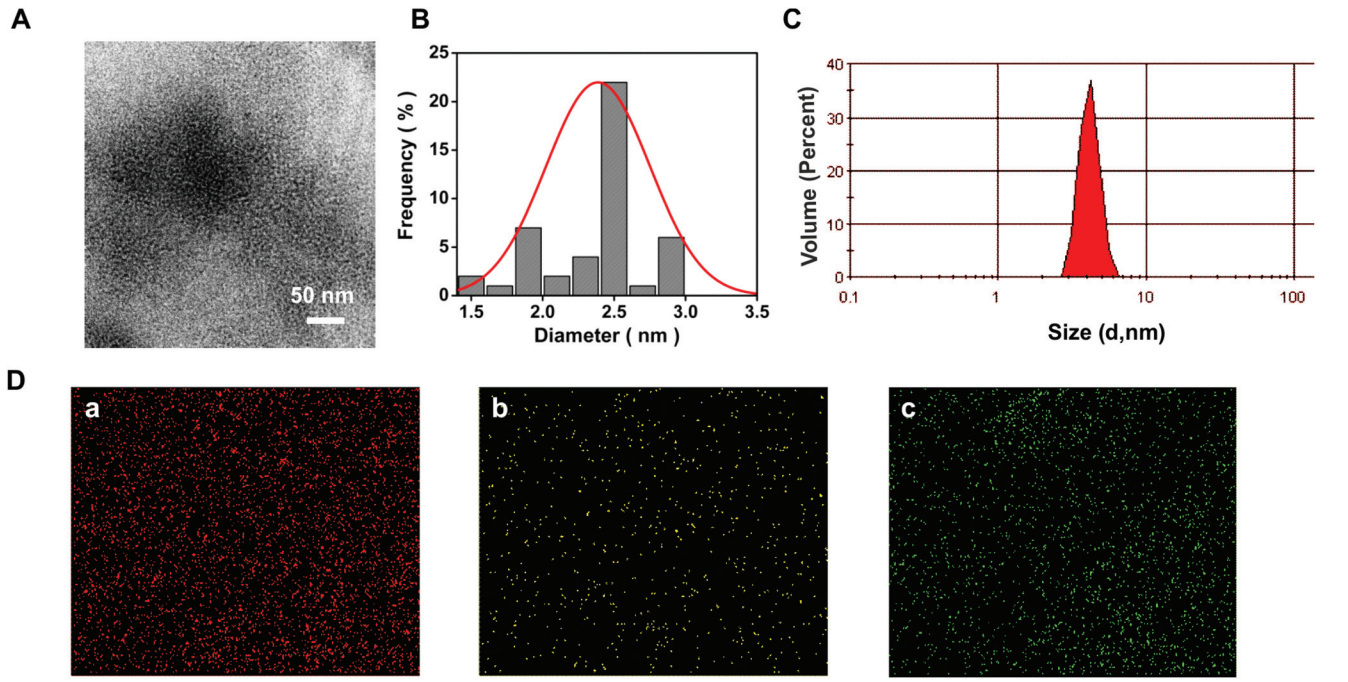

Fig. 2 (A) TEM image of CDs. (B) Size distribution histogram of CDs as determined by TEM. (C) DLS spectrum (size distribution by volume) of aqueous suspension of CDs. (D) Elemental mapping of CDs. (a–c) Individual elemental distribution (red for carbon, yellow for nitrogen and green for oxygen).

groups, which corroborates well with the EDS data (Table S2†). FTIR spectrum was further recorded to ascertain the exact chemical composition of CDs (Fig. 3(B)). Overlapping O–H/N–H stretching bands were detected at 3432 cm^{-1},[26] whereas peaks at 2837 cm^{-1} and 804 cm^{-1} corresponded to C–H stretching and bending vibrations.[18] Peaks at 2359 cm^{-1} and 2341 cm^{-1}

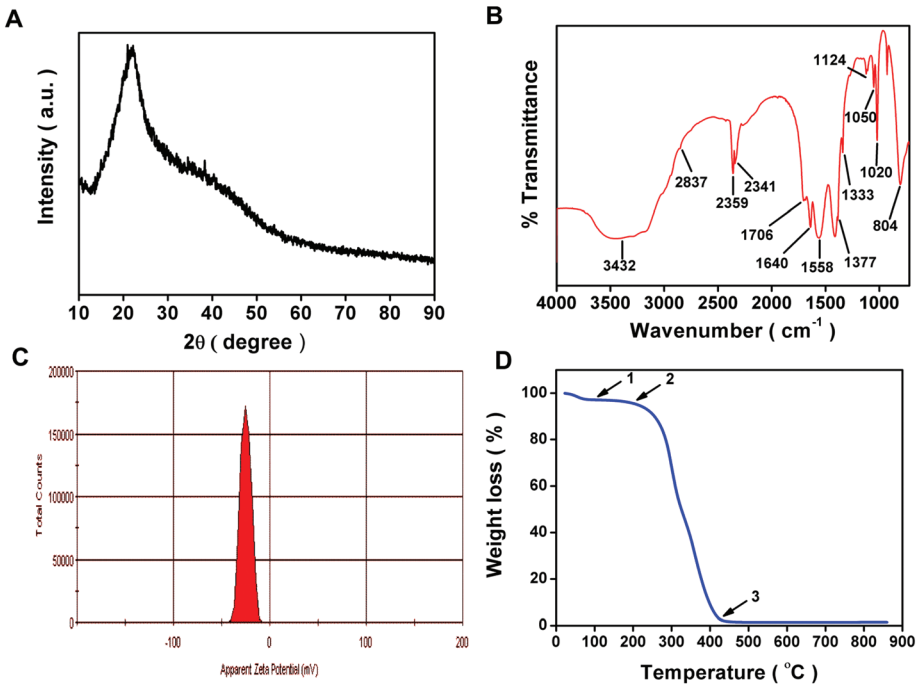

Fig. 3 (A) XRD pattern, (B) FTIR spectrum, (C) Zeta potential and (D) TGA analysis of CDs.

represented C–N stretching, while N–H deformation vibration was observed at 1558 cm^{-1}.[18,24] Furthermore, peaks at 1706 cm^{-1} and 1640 cm^{-1} corresponded to C=O and C=C stretch of carbon backbone of CDs. Notably, the peaks at 1377 cm^{-1}, 1333 cm^{-1} and 1020 cm^{-1} indicated asymmetric and symmetric vibrations of C–O–C, while peaks at 1124 cm^{-1} and 1050 cm^{-1} represented stretching and bending vibrations of C–O bonds in carboxyl groups.[18] The above investigations suggested that CDs were functionalized with hydroxyl, carboxylic, carbonyl and amino groups, derived from organic moieties in coriander leaves under hydrothermal conditions. These groups endow the CDs with excellent water solubility, with no signs of aggregation or loss of fluorescence after several months. The zeta potential of CDs was negative (−24.9 mV), due to the abundance of hydroxyl and carboxylic groups on the surface (Fig. 3(C)), in accordance with the elemental analysis and FTIR data.[18,24,31] The thermal stability of CDs was demonstrated by the TGA curve (Fig. 3(D)). The thermogram exhibited a three-step degradation pattern, with an initial weight loss of 3% at 100 °C due to elimination of water molecules or the moisture associated with CDs. A slight weight loss (7%) occurred between 100 and 200 °C, indicating thermal stability of CDs up to 200 °C. The final degradation step resulted in a significant weight loss (93%) in the range of 200–435 °C due to the gradual degradation of the surface functional groups of CDs. Beyond 435 °C the curve levelled off.[7,18,23] The effect of the solvent on the solubility and fluorescence intensity of CDs was investigated (Fig. S2†). CDs were found to be soluble in organic solvents such as *N*-dimethylformamide (DMF), dimethylsulfoxide (DMSO) and methanol. Further, it was observed that CDs had the highest fluorescence intensity in water, followed by methanol, DMSO and DMF, without any shift in the emission peaks. Due to high polarity of water compared to other organic solvents, CDs demonstrated superior fluorescence intensity in water. This multisolvent solubility could be attributed to the polar functional groups such as carboxyl and hydroxyl on the surface of CDs. Besides, pH dependence and the photostability of CDs were also studied. Fluorescence spectra of CDs were recorded at different pH values by adjusting the pH by 0.1 N solutions of HCl and NaOH. With an increase in pH in the range of 3–12, a steady increase in fluorescence intensity was recorded, with a maximum intensity at pH 12.0, beyond which no significant changes were found (Fig. 4(A)). Such pH dependent behaviour could be due to changes in the surface state of CDs due to the ionization of the carboxyl and hydroxyl groups as observed earlier.[4] The colloidal stability of CDs was studied in terms of changes in the zeta potential as a function of pH (Fig. 4(B)). The zeta potential value changed from 19.03 mV to −22.2 mV with an increase in pH. Higher zeta potential value favoured stable particle dispersion which is in accordance with the maximum emission observed at pH 12.0. Nonetheless, photostability studies indicate that CDs had a stable emission even after 2.5 h of continuous excitation. Fluorescence intensity decreased slightly (2.87%), representing a fairly good photostability (Fig. S3†).

3.1 Antioxidant activity

Antioxidant activity is a commonly used parameter to assess the ability of a material to scavenge or neutralize free radicals.

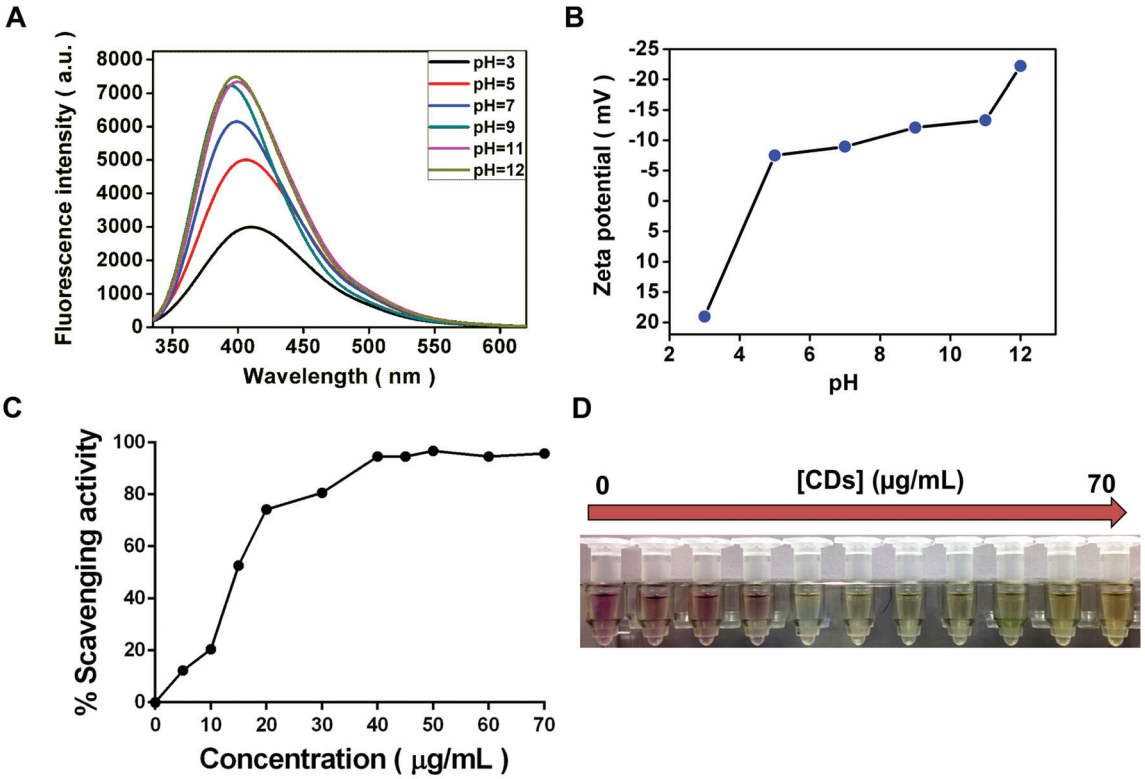

Fig. 4 (A) Dependence of Fluorescence emission of CDs on pH (λ_{ex} = 320 nm). (B) Variation in zeta potential of CDs as a function of pH. (C) DPPH free radical scavenging activity of CDs. (D) Photographic representation of bleaching of DPPH solution with a progressive increase in concentration of CDs.

There have been quite a few reports on the antioxidant activity of CDs.[29,30] DPPH based assay is one of the most commonly employed method to evaluate the antioxidant activity.[28] DPPH is a long-lived, nitrogen containing free radical which is deep purple in colour, which turns yellow as soon as it interacts with an antioxidant. Different concentrations of CDs were added to 50 μM methanolic DPPH solution. Decrease in absorbance at 517 nm was detected within minutes of incubation. From the results shown in Fig. 4(C), the radical scavenging activity of CDs was found to increase in a dose-dependent manner. As the concentration of CDs increased from 5 to 70 μg mL^{-1}, there was a subsequent increase in the scavenging activity from 12 to 94%. From the curve the EC_{50} value (amount of antioxidant required to decrease the concentration of DPPH by 50%) of CDs was estimated to be 15 μg mL^{-1}. Interestingly, the DPPH solution turned colourless to yellow with an increase in the concentrations of CD (Fig. 4(D)).

3.2 Ion sensing

In recent years, the development of fluorescence based sensors for selective and sensitive detection of metal ions has been pursued by various research groups.[32–35] In order to evaluate the ability of CDs obtained from coriander leaves for analytical purposes, their fluorescence intensity in the presence of different metal ions was monitored. Fig. 5(A) shows the relative change in the fluorescence intensity of CDs (0.1 mg mL^{-1}) in the presence of various metal ions (each at a concentration of 60 μM). Out of the 12 kinds of metal ions, Ag^{+}, Cu^{2+}, Hg^{2+} and Fe^{2+} caused slight reduction in the fluorescence intensity. This may be due to non-specific interactions between the functional groups and metal ions. In contrast, Fe^{3+} ions caused the strongest fluorescence quenching effect on CDs, thereby depicting higher selectivity towards Fe^{3+} ions than other metal ions.[36–39] This discrimination effect for Fe^{3+} ions originates due to exceptional coordination between Fe^{3+} ions and hydroxyl groups of CDs, similar to previous reports.[8–10] To explore the sensitivity of CDs towards Fe^{3+} ions, different concentrations of Fe^{3+} ions in the range of 0–60 μM were added in the CDs solution (0.1 mg mL^{-1}). Fig. 5(B) shows a steady decline in fluorescence intensity with increasing Fe^{3+} concentration. Fig. 5(C) further represents the relative fluorescence response of CDs (F_0/F) as a function of Fe^{3+} concentration. The fluorescence quenching efficiency can further be described by the Stern–Volmer plot depicting a perfect linear behaviour (linear correlation coefficient of 0.9874) in the concentration range 0–6 μM (inset in Fig. 5(C)). The equation for the same is as follows:

$$F_0/F = 0.07590X + 0.9780$$

where F_0 and F are the fluorescence intensities of CDs in the absence and presence of Fe^{3+} and X represents the concen-

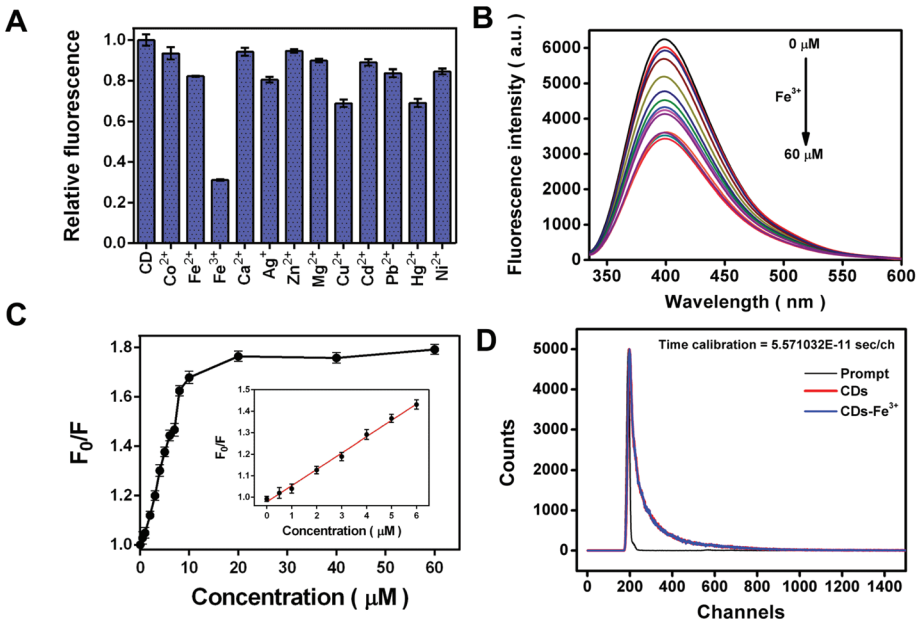

Fig. 5 (A) Fluorescence response of CDs in the presence of different metal ions in aqueous solution. (B) Fluorescence spectral quenching of CDs upon addition of various concentrations of Fe^{3+} (C) Relative fluorescence response of CDs (F_0/F) *versus* concentration of Fe^{3+} from 0 to 60 μM. Inset is the linear region from 0 to 6 μM. F_0 and F are the fluorescence intensities of CDs at 400 nm in the absence and presence of Fe^{3+}, respectively. (D) Fluorescence decay curve of CDs in the absence and presence of Fe^{3+} (λ_{ex} = 320 nm; λ_{em} = 400 nm).

tration of Fe^{3+}. On the basis of the above equation, the quenching constant, K_{sv} (slope of the linear fit) was calculated to be 7.590×10^4 mol^{-1} dm^{-3}. Likewise, the limit of detection was determined to be 0.4 μM based on the equation $3\sigma/m$, where σ is the standard deviation of blank signal (n = 4) and m is the slope of the linear fit. The detection limit is comparable to other reported values for Fe^{3+} detection by CDs.[8–10,40] Notably, this value is much lower than the maximum permissible level (5.36 μM) for Fe^{3+} in drinking water as per the guidelines laid down by World Health Organization (WHO).[41] Finally, fluorescence decay curve analysis was done to gain an insight into the fluorescence quenching mechanism of CDs (Fig. 5(D)). Decay curves of CDs and CD–Fe^{3+} overlapped suggesting negligible change in the fluorescence lifetime of CDs in the presence of Fe^{3+}. In addition, the average lifetime of CDs and CD–Fe^{3+} complex was calculated to be 5.94 ns and 5.90 ns, respectively which consisted of three lifetime components (Table S3†). Contrastingly, a small change in the lifetime of CDs ruled out the occurrence of dynamic quenching, thereby eliminating the possibility of electron transfer processes in CD–Fe^{3+} system.[8,40,42] EDS mapping (Fig. S4†) further shows the distribution of Fe^{3+} in CD–Fe^{3+} complex. Elemental maps depicted the presence of Fe^{3+} along with the major constituent elements of CDs. This suggests the uniform distribution of C, O and N with Fe^{3+} concentrated in specific areas. Since, CDs demonstrate a pH dependent response, the quenching effect of Fe^{3+} on CDs was explored at various pH values. Fig. S5† shows the pH dependent fluorescence response of the CD–Fe^{3+} complex. Under acidic conditions, low quenching efficiency was observed, due to protonation of surface carboxylic groups, resulting in weaker interactions in the CD–Fe^{3+} complex. In the pH range 7–9, a substantial decrease in fluorescence intensity (higher quenching efficiency) was observed owing to the deprotonation of surface carboxylic groups, thereby strengthening the interaction between Fe^{3+} and CDs. Conversely, at higher pH values lower quenching efficiency was observed again, which could be due to the complexation of Fe^{3+} by OH^- instead of CDs.[15,43] The above outcomes highlight the competence of CDs as Fe^{3+} nanosensor.

3.3 Biocompatibility and bioimaging

Cytotoxicity effects during imaging of cells play a key role in determining the applicability of nanoparticles as fluorescence imaging agents. Hence, it becomes imperative to assess the cytotoxicity of CDs before employing them for bioimaging. In this regard, the MTT assay was performed and the results are presented in Fig. 6(A). A549 cells did not show any decline in cell viability when the concentration of CDs was increased to 0.3 mg mL^{-1} with respect to control. Afterwards, a marginal decrease in cell viability was observed with increasing concentration of CDs. The survival rate was around 86% even at a high concentration of 1 mg mL^{-1}. Similarly, L-132 cells accounted for more than 85% cell viability at all the tested doses of CDs ranging from 0.1 to 1 mg mL^{-1}. Overall, the exposure of varied concentrations of CDs did not induce any serious cytotoxic effect in both A549 and L-132 cells. Essentially, the results portray the biocompatibility of CDs for bioimaging. As a proof-of-concept, A549 and L-132 cells were stained with CDs (Fig. 6(B)). Distinct green fluorescence inside the cells was observed upon subsequent cellular uptake of CDs

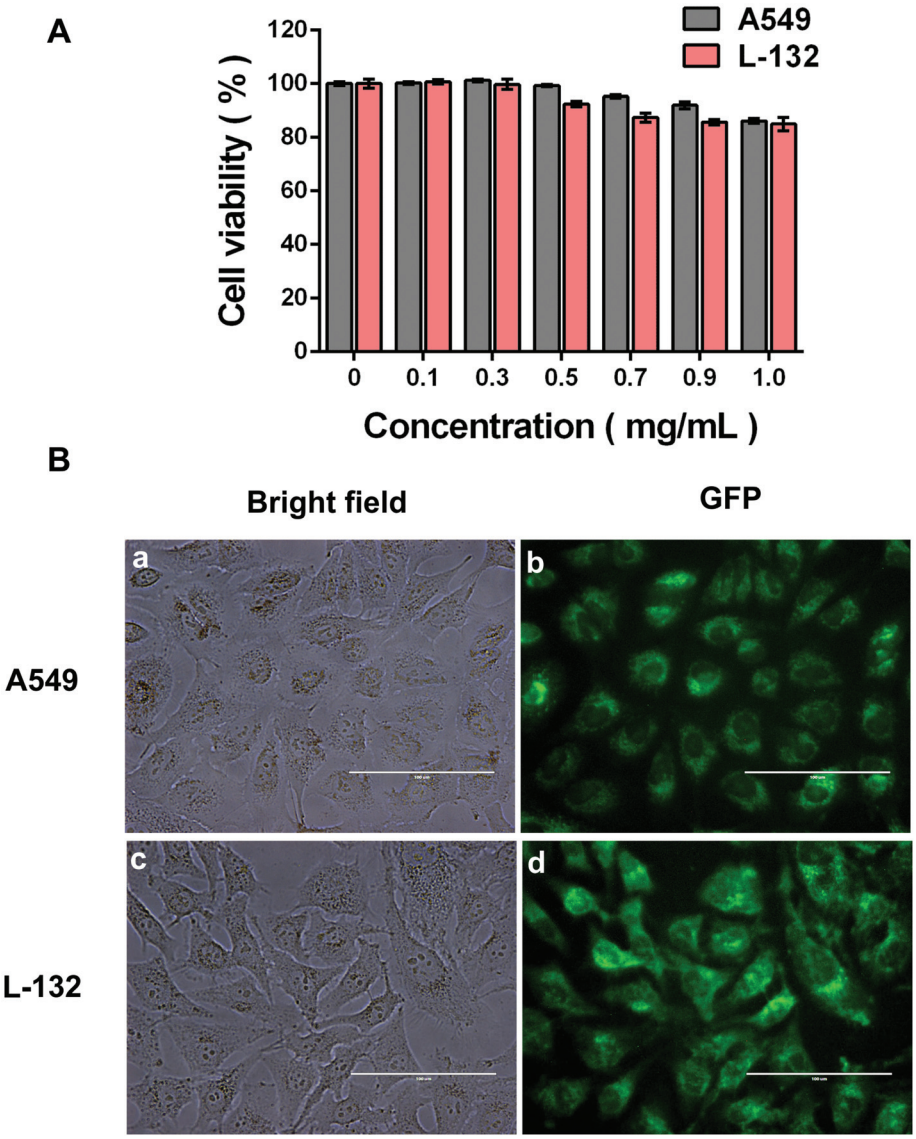

Fig. 6 (A) *In vitro* cell viability of A549 and L-132 cells treated with various concentrations of CDs as estimated by the MTT assay. The error bars represent mean ± S.E.M. of three individual experiments. (B) Representative fluorescence microscopic images of A549 (a and b) and L-132 (c and d) cells incubated with 0.5 mg mL^{-1} CDs. Scale bar: 100 μm. GFP Filter (λ_{ex} = 470 nm; λ_{em} = 525 nm).

(Fig. 6(b,d)). In addition, the bright field images of CDs treated cells indicate normal morphology of cells, endorsing the biocompatibility of CDs (Fig. 6(a,c)). For cellular uptake studies, Hoechst 33342 dye was used as a marker for nucleus and the cellular distribution of CDs was tracked in A549 and L-132 cell lines. As can be seen in Fig. S6,† CDs were ubiquitously distributed in the cytoplasm of cells, evident from the green fluorescence emanating around the nucleus. However, no co-localization of blue (Hoechst 33342) and green fluorescence (CDs) was observed, which underscores the fact that CDs were not able to penetrate inside the cell nucleus.[18,25,44] The quantification of cellular uptake of CDs in A549 and L-132 cells was done by determining the percentage of fluorescent cells using a flow cytometer with reference to control cells (Fig. 7). The fluorescence signal originating from CDs stained cells was strong enough to be detected by flow cytometer, while the cells not treated with CDs with insignificant background fluorescence were used as control. On closer inspection, an increase in the intracellular fluorescence intensity of CDs (percentage of fluorescent cells) was observed in both the cell types with an increase in concentration of CDs, thereby indicating concentration dependent cellular uptake. For the A549 treated cells, the percentage of fluorescent cells increased from 35.8% to 69.4% with an increase in the concentration of CDs (Fig. 7(b–c)). On the other hand, the percentage of fluorescent cells in L-132 treated cells also increased correspondingly from 59.7% to 82.9% in a dose-dependent manner (Fig. 7(e–f)). Evidently, there were marked differences in cellular uptake

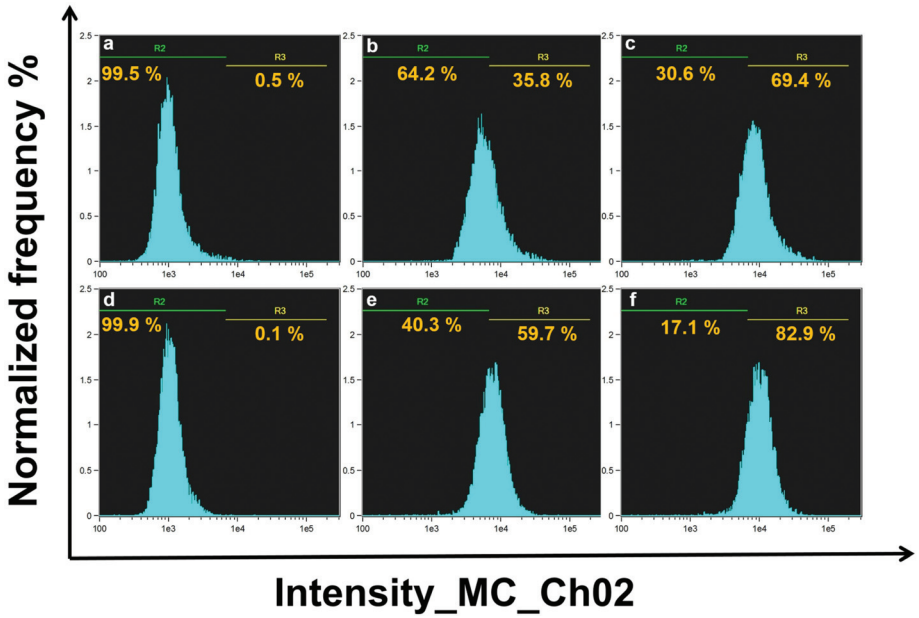

Fig. 7 Flow cytometric analysis of cellular uptake of CDs in A549 and L-132 cells. Upper panel: (a) untreated and (b) 0.3 mg mL^{-1}, (c) 0.5 mg mL^{-1} CDs treated A549 cells. Lower panel: (d) untreated and (e) 0.3 mg mL^{-1}, (f) 0.5 mg mL^{-1} CDs treated L-132 cells.

between the two cell types at equivalent cell numbers. L-132 cells had higher cellular uptake of CDs than A549 cells at similar test doses, under same conditions.

4. Conclusion

In summary, we have devised a direct, green synthetic approach for synthesizing self-passivated CDs using coriander leaves as a herbal carbon source for the first time, without using any additional passivating agent for surface modification. The as-synthesized green fluorescent CDs had superior optical characteristics and demonstrated excitation, pH and solvent dependent emission behaviour. Also, the CDs had remarkable photostability and aqueous solubility, paving a way for their utilization in various applications. These CDs had inherent antioxidant potency, apart from having selective ion detection capability. Quenching of fluorescence of CDs in the presence of Fe^{3+} ions provides a platform for their quantitative sensing by monitoring the fluorescence emission intensity of CDs. Meanwhile, low cytotoxicity of CDs under *in vitro* conditions implies the possible use of CDs for bioimaging purposes. CDs were effectively taken up by normal as well as cancer cells and localized mainly in the cytoplasm, highlighting their immense potential as fluorescence imaging nanoprobes. Detection of fluorescence signal from the CDs stained cells by flow cytometer predicted subtle differences in cellular uptake of CDs, which are generally not detected by fluorescence microscopy. Overall, we have demonstrated the probable use of CDs for a myriad of practical applications.

Acknowledgements

We sincerely thank the Science and Engineering Research Board (no. SR/FT/LS-57/2012) and the Department of Biotechnology (no. BT/PR6804/GBD/27/486/2012), Government of India, for the financial support. AS is thankful to the Ministry of Human Resource Development, Government of India, for the fellowship. Department of Chemistry and Institute Instrumentation Centre, Indian Institute of Technology Roorkee are sincerely acknowledged for providing various analytical facilities.

References

1 H. Li, Z. Kang, Y. Liu and S.-T. Lee, *J. Mater. Chem.*, 2012, **22**, 24230–24253.
2 S. N. Baker and G. A. Baker, *Angew. Chem., Int. Ed.*, 2010, **49**, 6726–6744.
3 L. Cao, S.-T. Yang, X. Wang, P. G. Luo, J.-H. Liu, S. Sahu, Y. Liu and Y.-P. Sun, *Theranostics*, 2012, **2**, 295–301.
4 A. Sachdev, I. Matai and P. Gopinath, *RSC Adv.*, 2014, **4**, 20915–20921.
5 A. Sachdev, I. Matai, S. U. Kumar, B. Bhushan, P. Dubey and P. Gopinath, *RSC Adv.*, 2013, **3**, 16958–16961.
6 C. Liu, P. Zhang, X. Zhai, F. Tian, W. Li, J. Yang, Y. Liu, H. Wang, W. Wang and W. Liu, *Biomaterials*, 2012, **33**, 3604–3613.
7 Q. Wang, X. Huang, Y. Long, X. Wang, H. Zhang, R. Zhu, L. Liang, P. Teng and H. Zheng, *Carbon*, 2013, **59**, 192–199.
8 X. Gong, W. Lu, M. C. Paau, Q. Hu, X. Wu, S. Shuang, C. Dong and M. M. F. Choi, *Anal. Chim. Acta*, 2015, **861**, 74–84.

9 J. Wang, F. Peng, Y. Lu, Y. Zhong, S. Wang, M. Xu, X. Ji, Y. Su, L. Liao and Y. He, *Adv. Opt. Mater.*, 2014, **3**, 103–111.
10 X. Teng, C. Ma, C. Ge, M. Yan, J. Yang, Y. Zhang, P. C. Morais and H. Bi, *J. Mater. Chem. B*, 2014, **2**, 4631–4639.
11 G. Gedd, S. Pandey, M. L. Bhaisare and H. F. Wu, *RSC Adv.*, 2014, **4**, 38027–38033.
12 P. Mondal, K. Ghosal, S. K. Bhattacharyya, M. Das, A. Bera, D. Ganguly, P. Kumar, J. Dwivedi, R. K. Gupta, A. A. Martí, B. K. Gupta and S. Maiti, *RSC Adv.*, 2014, **4**, 25863–25866.
13 C. Liu, P. Zhang, F. Tian, W. Li, F. Li and W. Liu, *J. Mater. Chem.*, 2011, **21**, 13163–13167.
14 L. Hu, Y. Sun, S. Li, X. Wang, K. Hu, L. Wang, X. Liang and Y. Wu, *Carbon*, 2014, **67**, 508–513.
15 H. Huang, Y. Xu, C. J. Tang, J. R. Chen, A. J. Wang and J. J. Feng, *New J. Chem.*, 2014, **38**, 784–789.
16 A. Barati, M. Shamsipur, E. Arkan, L. Hosseinzadeh and H. Abdollahi, *Mater. Sci. Eng., C*, 2015, **47**, 325–332.
17 L. Wang and H. S. Zhou, *Anal. Chem.*, 2014, **86**, 8902–8905.
18 V. N. Mehta, S. Jha, R. K. Singhal and S. K. Kailasa, *New J. Chem.*, 2014, **38**, 6152–6160.
19 S. L. Hu, K. Y. Niu, J. Sun, J. Yang, N. Q. Zhao and X. W. Du, *J. Mater. Chem.*, 2009, **19**, 484–488.
20 H. Jiang, F. Chen, M. G. Lagally and F. S. Denes, *Langmuir*, 2010, **26**, 1991–1995.
21 S. C. Ray, A. Saha, N. R. Jana and R. Sarkar, *J. Phys. Chem. C*, 2009, **113**, 18546–18551.
22 S. Sahu, B. Behera, T. K. Maiti and S. Mohapatra, *Chem. Commun.*, 2012, **48**, 8835–8837.
23 A. Mewada, S. Pandey, S. Shinde, N. Mishra, G. Oza, M. Thakur, M. Sharon and M. Sharon, *Mater. Sci. Eng., C*, 2013, **33**, 2914–2917.
24 L. Zhu, Y. Yin, C. F. Wang and S. Chen, *J. Mater. Chem. C*, 2013, **1**, 4925–4932.
25 L. Shi, X. Li, Y. Li, X. Wen, J. Li, M. M. F. Choi, C. Dong and S. Shuang, *Sens. Actuators, B*, 2015, **210**, 533–541.
26 S. Y. Park, H. U. Lee, E. S. Park, S. C. Lee, J. W. Lee, S. W. Jeong, C. H. Kim, Y. C. Lee, Y. S. Huh and J. Lee, *ACS Appl. Mater. Interfaces*, 2014, **6**, 3365–3370.
27 U. K. Sukumar, B. Bhushan, P. Dubey, I. Matai, A. Sachdev and P. Gopinath, *Int. Nano Lett.*, 2013, **3**, 45–53.
28 K. Pyrzynska and A. Pekal, *Anal. Methods*, 2013, **5**, 4288–4295.
29 B. Das, P. Dadhich, P. Pal, P. K. Srivas, K. Bankoti and S. Dhara, *J. Mater. Chem. B*, 2014, **2**, 6839–6847.
30 M. D. Purkayastha, A. K. Manhar, V. K. Das, A. Borah, M. Mandal, A. J. Thakur and C. L. Mahanta, *J. Agric. Food Chem.*, 2014, **62**, 4509–4520.
31 Z. Liang, L. Zeng, X. Cao, Q. Wang, X. Wang and R. Sun, *J. Mater. Chem. C*, 2014, **2**, 9760–9766.
32 K. Z. Kamali, A. Pandikumar, G. Sivaraman, H. N. Lim, S. P. Wren, T. Sund and N. M. Huang, *RSC Adv.*, 2015, **5**, 17809–17816.
33 G. Sivaraman, T. Anand and D. Chellappa, *ChemPlusChem*, 2014, **79**, 1761–1766.
34 G. Sivaraman, T. Anand and D. Chellappa, *Analyst*, 2012, **137**, 5881–5884.
35 G. Sivaraman and D. Chellappa, *J. Mater. Chem. B*, 2013, **1**, 5768–5772.
36 X. Bao, J. Shi, X. Nie, B. Zhou, X. Wang, L. Zhang, H. Liao and T. Pang, *Bioorg. Med. Chem.*, 2014, **22**, 4826–4835.
37 T. M. Geng, R. Y. Huang and D. Y. Wu, *RSC Adv.*, 2014, **4**, 46332–46339.
38 D. En, Y. Guo, B. T. Chen, B. Dong and M. J. Peng, *RSC Adv.*, 2014, **4**, 248–253.
39 G. Sivaraman, V. Sathiyaraja and D. Chellappa, *J. Lumin.*, 2014, **145**, 480–485.
40 S. Zhu, Q. Meng, L. Wang, J. Zhang, Y. Song, H. Jin, K. Zhang, H. Sun, H. Wang and B. Yang, *Angew. Chem., Int. Ed.*, 2013, **52**, 3953–3957.
41 WHO, World Health Organization Switzerland, 2011, **4**, 226.
42 Y. Zhai, Z. Zhu, C. Zhu, J. Ren, E. Wang and S. Dong, *J. Mater. Chem. B*, 2014, **2**, 6995–6999.
43 F. Yan, Y. Zou, M. Wang, X. Mu, N. Yang and L. Chen, *Sens. Actuators, B*, 2014, **192**, 488–495.
44 A. Sachdev, I. Matai and P. Gopinath, *J. Mater. Chem. B*, 2015, **3**, 1217–1229.